Title
Scaling of the anomalous Hall effect in lower conductivity regimes

Journal
EPL (Europhysics Letters), 114(5)

ISSN
0295-5075

Authors
Karel, J
Bordel, C
Bouma, DS
et al.

Publication Date
2016-06-01

DOI
10.1209/0295-5075/114/57004

Peer reviewed

A Letters Journal Exploring the Frontiers of Physics

June 2016

EPL, **114** (2016) 57004
doi: 10.1209/0295-5075/114/57004

www.epljournal.org

Scaling of the anomalous Hall effect in lower conductivity regimes

J. Karel[1,2(a)], C. Bordel[2,3,4], D. S. Bouma[3], A. de Lorimier-Farmer[3], H. J. Lee[3] and F. Hellman[1,2,3]

[1] *Department of Materials Science and Engineering, University of California - Berkeley, CA 94720, USA*
[2] *Materials Science Division, Lawrence Berkeley National Lab - Berkeley, CA 94720, USA*
[3] *Physics Department, University of California - Berkeley, CA 94720, USA*
[4] *Groupe de Physique des Matériaux, UMR CNRS 6634, Université de Rouen - 76801 St. Etienne du Rouvray, France*

received 28 January 2016; accepted in final form 12 June 2016
published online 7 July 2016

PACS 73.50.-h – Electronic transport phenomena in thin films
PACS 73.61.Jc – Amorphous semiconductors; glasses
PACS 73.50.Jt – Galvanomagnetic and other magnetotransport effects (including thermomagnetic effects)

Abstract – The scaling of the anomalous Hall effect (AHE) was investigated using amorphous and epitaxial Fe_xSi_{1-x} ($0.43 < x < 0.71$) magnetic thin films by varying the longitudinal conductivity (σ_{xx}) using two different approaches: modifying the carrier mean free path (l) with chemical or structural disorder while holding the carrier concentration (n_h) constant or varying n_h and keeping l constant. The anomalous Hall conductivity (σ_{xy}), when suitably normalized by magnetization and n_h, is shown to be independent of σ_{xx} for *all* samples. This observation suggests a primary dependence on an intrinsic mechanism, unsurprising for the epitaxial high conductivity films where the Berry phase curvature mechanism is expected, but remarkable for the amorphous samples. That the amorphous samples show this scaling indicates a local atomic level description of a Berry phase, resulting in an intrinsic AHE in a system that lacks lattice periodicity.

The consideration of topology has recently led to the emergence of new exotic physics; topological insulators and Weyl semimetals are two classes of materials where unique properties arise due to the topology of the electronic band structure [1–5]. Since its discovery, the Berry phase has helped explain diverse phenomena in condensed matter physics, including polarization, the spin and quantum Hall effect, contributions to orbital magnetism, and the intrinsic contribution to the anomalous Hall effect (AHE) in ferromagnets, which can be interpreted in terms of a Berry phase curvature in momentum space [6,7].

The AHE in ferromagnets arises from several origins. To parse these individual contributions, a unifying theory has been proposed based on the longitudinal conductivity, σ_{xx}, or more specifically, the carrier lifetime τ [6,8]. The theory splits the anomalous Hall conductivity (σ_{xy}) into three regions. In the clean limit ($\sigma_{xx} > 10^6 \Omega^{-1}\,\mathrm{cm}^{-1}$) at low temperature T, the skew-scattering mechanism, which is due to asymmetric spin scattering from impurities with spin-orbit coupling, dominates, and $\sigma_{xy} \propto \sigma_{xx}$ [6,9,10]. In the second regime ($10^4\,\Omega^{-1}\mathrm{cm}^{-1} < \sigma_{xx} < 10^6\,\Omega^{-1}\mathrm{cm}^{-1}$), the intrinsic (Berry phase) mechanism is the dominant contribution to σ_{xy}. This contribution is associated with spin-orbit coupling which causes a gap to open at band anti-crossing points in the electronic band structure. If the Fermi energy lies near these points, a large Berry phase curvature occurs, giving rise to σ_{xy} [6,11]. In this regime, σ_{xy} = constant. Numerous experimental results have verified the dependences of σ_{xy} in these two regimes for, *e.g.*, Fe, Co, Ni, and Gd [12–14]. The low σ_{xx} regime ($\sigma_{xx} < 10^4\,\Omega^{-1}\mathrm{cm}^{-1}$, $\rho_{xx} > 100\,\mu\Omega\mathrm{cm}$) is less well understood. Onoda *et al.* theoretically calculated $\sigma_{xy} \propto \sigma_{xx}^{1.6}$ by changing impurity concentration; in that work, magnetization (M) is assumed to not change [8]. Similarly, experimental results from chalcogenide-spinel structures ($CuCr_2Se_{4-x}Br_x$) [13,15], Co-ZnO [16], $Ti_{1-x}Co_xO_{2-\delta}$ (oxygen deficiency δ) [17], Fe_3O_4 and $Fe_{3-x}Zn_xO_4$ [18] show $\sigma_{xy} \propto \sigma_{xx}^n$ where $1.5 < n < 1.8$; in these works, M was not considered in the analysis.

The present work specifically investigates the two lower σ_{xx} regimes. This study was performed at low T with two different approaches to change σ_{xx}: i) modifying mean free path, l, using either chemical or structural order and holding the number of charge carriers (n_h) roughly constant or ii) changing n_h and keeping l constant. Thin films of

[(a)] Present address: Max-Planck-Institut für Chemische Physik fester Stoffe - Dresden, 01187, Germany.

Fe_xSi_{1-x} ($0.43 < x < 0.71$) are an ideal system for these investigations since deposition techniques allow access to both structural and chemical order [19,20]. In the narrow composition range $0.67 < x < 0.71$, it is possible to fabricate both amorphous films and epitaxial films with different chemical order, $D0_3$ or B2; $D0_3$ is more chemically ordered while B2 is less. Due to these differences, significant changes in l can be realized while n_h remains roughly constant. Moreover, amorphous films can be fabricated over a wide composition range, where l is constant and n_h changes.

Amorphous and epitaxial Fe_xSi_{1-x} thin films ($0.43 < x < 0.71$; 70–100 nm thickness) were grown at room temperature and at 300 °C on (100) MgO and amorphous-SiN_x-on-Si substrates by electron-beam co-evaporation of Fe and Si. The structure of all films was measured using x-ray diffraction (XRD) and high-resolution cross-section transmission electron microscopy (HRXTEM) [19,20]. Films with $x = 0.71$ and $x = 0.67$ grown at 300 °C on MgO were epitaxial with $D0_3$ and B2 structure, respectively. For films with $x = 0.43$–0.71 grown at room temperature on SiN_x/Si substrates, no peaks were observed in XRD. HRXTEM imaging was performed on two samples, $x = 0.55$ and 0.67. The $x = 0.67$ sample displayed a predominantly amorphous structure (80% volume fraction) with some embedded nanocrystals (∼20% volume fraction, ∼5 nm diameter). The $x = 0.55$ sample was fully amorphous. Samples were patterned into Hall bars (40 μm × 120 μm) with 6 current-voltage ($I - V$) leads using standard photolithography and wet etch techniques for Hall effect, magnetoresistance and resistivity measurements. Magnetization (M) as a function of T and H was measured using a Quantum Design SQUID MPMS. Further sample preparation, characterization and measurement details can be found in the supplementary information.

Figure 1(a) shows longitudinal resistivity (ρ_{xx}) as a function of T for epitaxial or amorphous films with different x. The epitaxial films display typical metallic behavior: increasing ρ_{xx} with increasing T, *i.e.* a positive temperature coefficient of resistivity (α) at all T. $\rho_{xx}(T)$ for the amorphous films is almost T-independent but depends strongly on x. For these films, the mean free path is approximately the interatomic distance and nearly temperature independent, leading to a small α, which changes sign from positive to negative with increasing x Previous work has shown that α correlates linearly with ρ_{xx}; in the present data, α crosses from positive to negative at approximately 150 $\mu\Omega$cm, typical for amorphous metals [21,22]. The dependence of ρ_{xx} on x and its independence of T indicates that the number of charge carriers decreases as x decreases. In the $x = 0.43$ sample, a clear minimum in $\rho_{xx}(T)$ at $T = 18$ K is observed; this minimum is also present at $T = 24$ and 27 K for $x = 0.45$ and 0.48, respectively. A resistivity minimum such as the one found here can result from the Kondo effect or resonant impurity scattering [23,24].

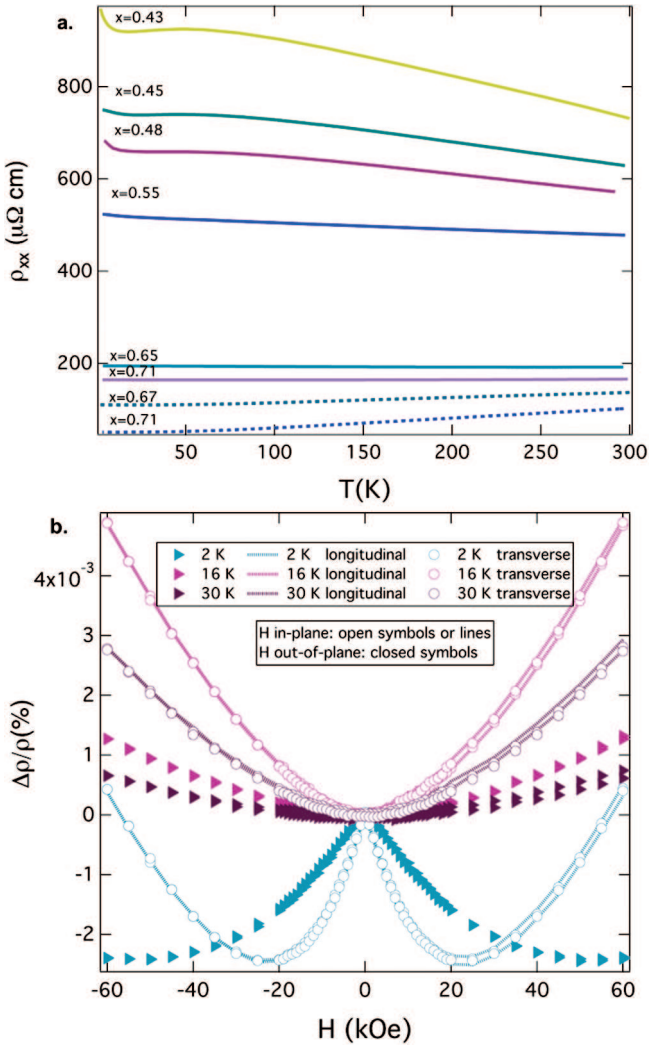

Fig. 1: (Colour online) (a) ρ_{xx}, *vs.* T for amorphous (solid lines) and epitaxial films (dashed lines) and (b) MR $\Delta\rho/\rho, [\Delta\rho = \rho(H) - \rho(0)]/\rho(H)$ *vs.* applied field with H applied out of the film plane (closed symbols), with H applied in the film plane and parallel to I (dashed lines) and with H in the film plane and perpendicular to I (open symbols) at various T for amorphous $x = 0.43$.

Magnetoresistance (MR) measurements with H applied perpendicular to the film and to the current I and H applied in the film plane and either parallel or perpendicular to I were performed at various T on the amorphous $x = 0.43$ sample shown in fig. 1(b). The magnitude of the MR is small. At 16 and 30 K, all MR shows a positive H^2 dependence, typical for metals [25]. At 2 K, the out-of-plane MR is negative, and the in-plane MR switches from negative to positive with increasing H. Negative magnetoresistance can result from weak localization [26] or can be found in systems that exhibit resonant impurity scattering [23]. In the latter, the negative MR is attributed to interactions between local moments and conduction electrons: the magnetic field aligns local moments, reducing the disorder seen by conduction electrons.

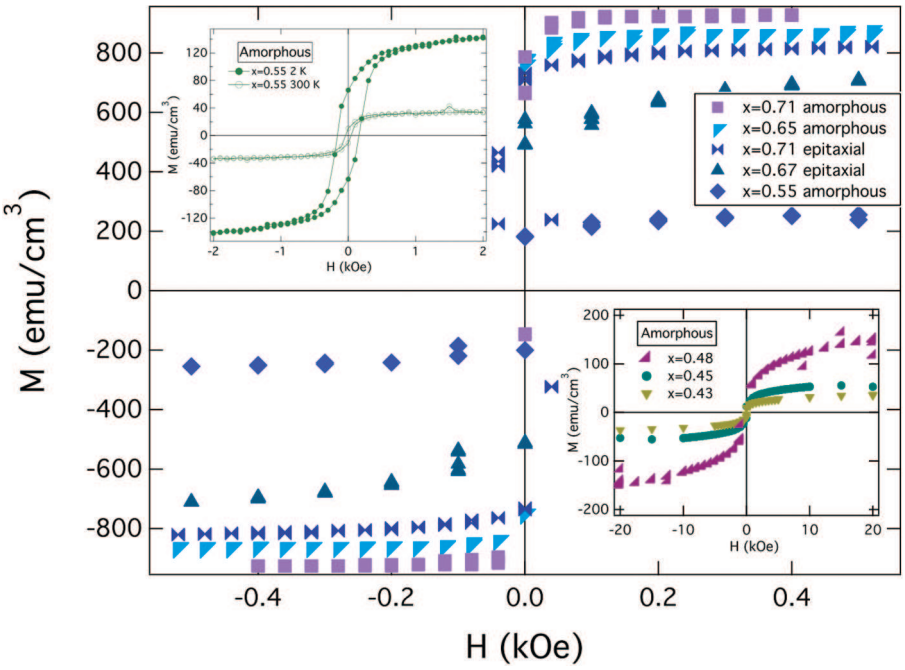

Fig. 2: (Colour online) In-plane $M(H)$ at 2 K for amorphous and epitaxial films. The top left inset shows in-plane $M(H)$ at 2 K and 300 K for amorphous $x = 0.53$. The bottom right inset shows $M(H)$ of amorphous $x = 0.43$–0.48 films on an expanded scale. The T-independent diamagnetic contribution (visible at high fields, and the same for H in-plane or out-of-plane) has been removed from all the data.

Figure 2 shows in-plane $M(H)$ curves at 2 K for amorphous and epitaxial films with various x; the bottom right inset displays the three lowest Fe concentration amorphous samples. Square $M(H)$ loops are observed for all $x \geq 0.55$, indicating the samples are ferromagnetic. The top left inset of fig. 2 displays an exemplary curve for an amorphous sample with $x = 0.53$, and demonstrates hysteresis in $M(H)$ at both 2 and 300 K. For a given x, M is $\sim$ 20% larger in the amorphous film than in the crystalline film, as discussed in references [19,20]; chemical order (either B2 or $D0_3$) in the epitaxial films leads to more Fe-Si pairs and thus a reduction in M. Ferromagnetism occurs in the amorphous Fe_xSi_{1-x} system at $x \sim 0.40$, consistent with previous work [27]; the amorphous samples with $x = 0.43$–0.48 are near this critical composition, and lack squareness in $M(H)$. However, magnetic remanence and M at all H larger than for a paramagnet (for reasonable values of S) are observed, indicating that these samples have ferromagnetic interactions, and are not simply paramagnetic; we therefore call these samples weakly ferromagnetic (meaning low M and low T_c). The in-plane and out-of-plane $M(H)$ curves are not significantly different for these amorphous $x = 0.43$–0.48 samples, consistent with low M which leads to low shape anisotropy.

The magnetic field dependence (H perpendicular to film plane) of transverse resistivity (ρ_{xy}) at 2 K is shown in fig. 3. The Hall effect in ferromagnets has two contributions, one from the ordinary Hall effect (OHE) due to the Lorentz force, proportional to H, and one from the AHE due to asymmetric scattering, proportional to the perpendicular component of M (M_z). The equation describing this effect takes the form

$$\rho xy(\text{total}) = \rho xy(\text{OHE}) + \rho xy(\text{AHE}) = R_0 H + R_s M_z. \quad (1)$$

Here, R is the ordinary Hall coefficient ($R_0 = \pm 1/ne$), and R_s is the anomalous Hall coefficient. From $\rho_{xy}(H)$ at large H (where $M(H)$ has saturated) the ordinary Hall effect can be used to determine carrier concentration. The positive slope of $\rho_{xy}(H)$ shows that the primary charge carriers are holes, consistent with findings for Fe [28] and Fe_3Si [29]. Since $M(H)$ is not square for $x = 0.43$, 0.45 and 0.48, R_0 was extracted iteratively using the full relation in eq. (1). For $x = 0.43$, 0.45 and 0.48, this procedure gives n_h at 2 K as approximately 5.6×10^{21} cm^{-3}, 1.5×10^{22} cm^{-3} and 1.6×10^{22} cm^{-3}, respectively[1]. For higher x, $\partial\rho_{xy}/\partial H$ is too small to measure and a linear extrapolation of n_h was made based on reported values for $x = 1.0$ and 0.75 [28,29].

Figure 3 shows that ρ_{xy}(AHE) is many times larger for the amorphous films than the epitaxial films with the same or similar compositions, an effect also seen in limited transport studies at low temperature of polycrystalline and amorphous vapor-quenched Fe [30]. In particular, we highlight the comparison between the $x = 0.71$ epitaxial and $x = 0.71$ amorphous samples where ρ_{xy} and ρ_{xx} are significantly larger in the latter, even though both

[1]Due to the small slope in $M(H)$ present at high H, R_0 was determined by calculating ρ_{xy}(total) using $M(H)$ and iterating R_0 and R_s until the calculated and experimental curves matched.

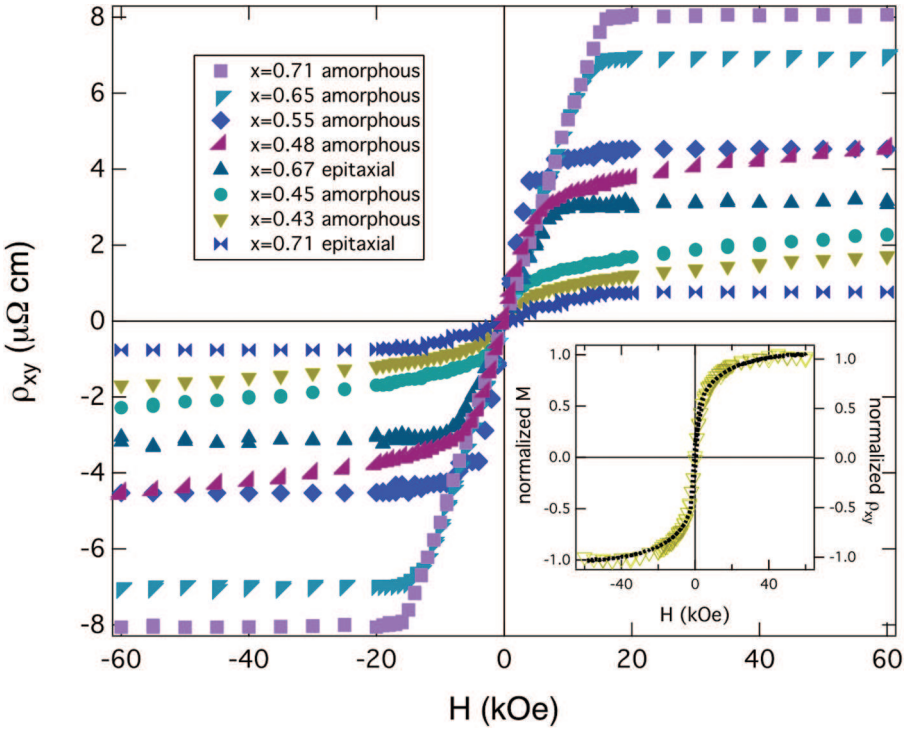

Fig. 3: (Colour online) ρ_{xy} *vs.* H at 2 K for amorphous and epitaxial films of various x. $\rho_{xy}(H) \propto M_z(H)$ for all samples, showing dominance of AHE. The inset shows normalized out-of-plane magnetization (black line) and normalized ρ_{xy}(AHE) (yellow open triangles) at 2 K for $x = 0.43$ with ρ_{xy}(OHE) subtracted.

samples have roughly the same M and n_h. The inset of fig. 3 shows normalized out-of-plane magnetization and normalized ρ_{xy}(AHE) for the $x = 0.43$ sample. The slope due to the ordinary Hall effect has been removed from ρ_{xy}(total) to show that the AHE scales with M_z. Similar behavior was observed for all samples. ρ_{xy} was also measured at higher T (*i.e.* 16, 30, 300 K) for some samples; the magnitude of ρ_{xy} decreased compared to the 2 K value, quantitatively consistent with its scaling with M_z. We also note that ρ_{xy} is far larger for epitaxial $x = 0.67$ than for epitaxial $x = 0.71$, a result that we attribute primarily to the difference in chemical order (B2 *vs.* $D0_3$) which leads to increased scattering for the B2 $x = 0.67$ sample, since the difference in n_h is small.

The anomalous Hall conductivity is calculated from $\sigma_{xy}(\text{AHE}) = \rho_{xy}(\text{AHE})/(\rho_{xx}^2 + \rho_{xy}(\text{AHE})^2) \sim \rho_{xy}(\text{AHE})/\rho_{xx}^2$ [18]. ρ_{xy}(AHE) is obtained by extrapolating ρ_{xy}(total) to zero field. Since $\sigma_{xy}(\text{AHE}) \propto \rho_{xy}(\text{AHE})$, both are $\propto M_z$ [31]. In general, M changes as a function of composition and structure so (as in refs. [10,31]), it is essential to separate the dependence of σ_{xy} on M from changes in impurities that lead to changes in σ_{xx}. Figure 4(a) shows σ_{xy}/M_z *vs.* σ_{xx} at 2 K for the Fe_xSi_{1-x} thin films investigated and a series of $Ga_{1-y}Mn_yAs$ samples at 15 K from [32]. The epitaxial samples and the amorphous sample with $x = 0.71$ display σ_{xy}/M_z = constant while the lower σ_{xx} amorphous samples show $\sigma_{xy}/M_z \propto \sigma_{xx}^{1.3}$, qualitatively similar to the $Ga_{1-y}Mn_yAs$ data.

We first discuss the regime where σ_{xy}/M_z is constant. It is notable that this occurs despite differences of more than a factor of 3 in ρ_{xx} and about a factor of 10 in ρ_{xy}; this is because σ_{xy} is proportional to ρ_{xy}/ρ_{xx}^2. In this σ_{xx} range, the change in n_h is very small, while l varies significantly first by changing chemical order from $D0_3$ ($x = 0.71$) to B2 ($x = 0.67$) and then structural order (amorphous $x = 0.71$). Despite these structural changes and differences in magnetization, σ_{xy}/M_z is constant. Two mechanisms could give rise to this scaling: the intrinsic mechanism previously discussed and the side-jump mechanism. The side-jump mechanism, which is due to asymmetric spin scattering from impurities with spin-orbit coupling, contributes much less to the AHE in this σ_{xx} regime ($10^4\,\Omega^{-1}\text{cm}^{-1} < \sigma_{xx} < 10^6\,\Omega^{-1}\text{cm}^{-1}$) [8,13]. In particular, calculations of bcc Fe show the intrinsic contribution comprises roughly 75% of the total signal; for this reason, we suggest it is also the dominant mechanism in these $x \sim 0.7$ Fe_xSi_{1-x} samples [33]. Most notably fig. 4(a) shows that the amorphous $x = 0.71$ sample falls in this scaling regime, indicating that the AHE for this sample also lies in the intrinsic regime.

Moreover, we suggest *the same intrinsic mechanism* is responsible for the behavior of the AHE in the low σ_{xx}(lower x) range. These amorphous samples ($0.43 < x < 0.65$) exhibit a $\sigma_{xy}/M_z \propto \sigma_{xx}^{1.3}$ scaling in fig. 4(a). Note that plotting σ_{xy} *vs.* σ_{xx} results in $\sigma_{xy} \propto \sigma_{xx}^{3.1}$, significantly different from the $\sigma_{xy} \propto \sigma_{xx}^n$ ($1.6 < n < 1.8$) relationship found in [13,18]. Since the carrier

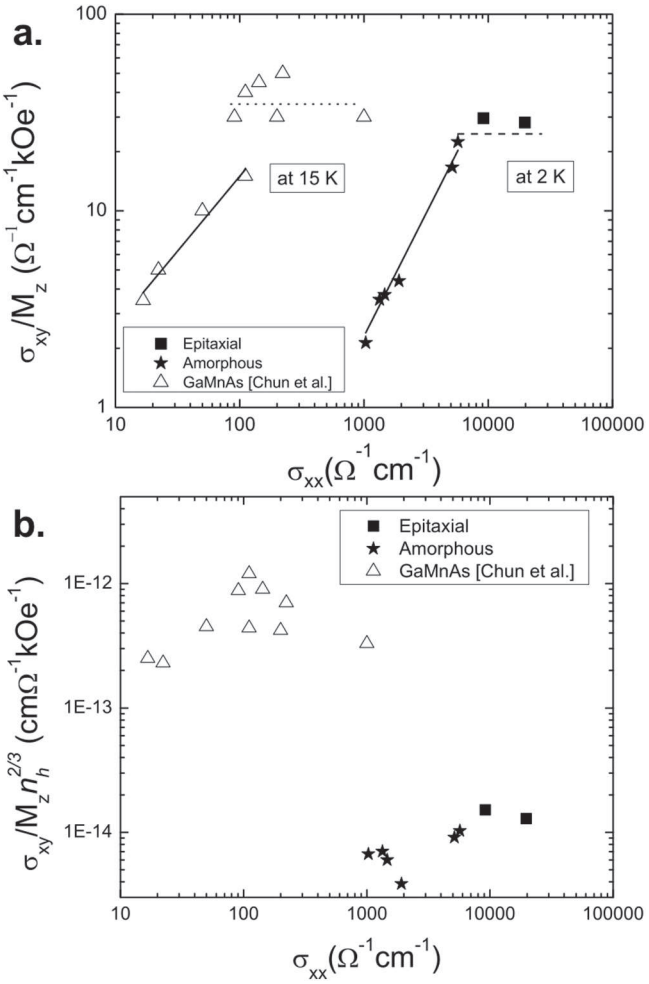

Fig. 4: (a) σ_{xy}/M_z *vs.* σ_{xx} for amorphous and epitaxial Fe_xSi_{1-x} thin films and GaMnAs thin films from [32]. The solid lines are fits to the low σ_{xx} data; $\sigma_{xy}/M_z \propto \sigma_{xx}^n$ with $n = 1.3$ (Fe_xSi_{1-x}) and 0.8 ($Ga_{1-y}Mn_yAs$). The horizontal dashed lines are a guide to the eye. (b) $\sigma_{xy}/M_z n_h^{2/3}$ *vs.* σ_{xx} for the same samples.

concentration was explicitly modified in this σ_{xx} range and the unifying theory was developed based on a change in τ [7,8], we suggest that to understand AHE, the dependence on n_h must be removed. Specifically, in fig. 4(b) the data were normalized by $n_h^{2/3}$, a free electron type dependence that can be derived from $\sigma_{xx} = [n^{2/3}e^2\,l]/[\hbar(3\pi^2)^{1/3}]$ when l is roughly constant. Removing the $n_h^{2/3}$ dependence results in a constant value for *all* the samples, suggesting that the intrinsic mechanism is dominant in this regime as well.

The scaling observed here for Fe_xSi_{1-x} is similar to that seen by Chun *et al.* in $Ga_{1-y}Mn_yAs$, where n_h was varied to change σ_{xx} [32]. In that report, the authors normalized σ_{xy} by either M_z or $n_h^{2/3}$; this analysis led to two distinct scaling regimes. The metallic samples showed an intrinsic AHE (also verified by [34]), where the magnitude of $\sigma_{xy}/n_h^{2/3}$ quantitatively corresponded to the strength of the exchange coupling between the local moments and conduction electrons (J_{pd}) predicted theoretically. The more insulating samples ($\sigma_{xx} < 10^2\,\Omega^{-1}\mathrm{cm}^{-1}$) displayed a linear scaling with σ_{xx} for both σ_{xy}/M_z and $\sigma_{xy}/n_h^{2/3}$, which was attributed to unspecified extrinsic origins. Figure 4(b) shows that normalizing σ_{xy} by *both* M_z and $n_h^{2/3}$ produces a nearly constant value for all $Ga_{1-y}Mn_yAs$ samples from Chun *et al.*, similar to our Fe_xSi_{1-x} results. While $\sigma_{xy}/M_z n_h^{2/3}$ is constant for both Fe_xSi_{1-x} and $Ga_{1-y}Mn_yAs$, the latter is two orders of magnitude larger than the former. We suggest this result originates from differences in J_{pd}, which is larger in $Ga_{1-y}Mn_yAs$ due perhaps to more localized wave functions (indicated by reduced σ_{xx}).

In conclusion, an anomalous Hall effect was observed in all samples; for comparable x, n_h, and M, ρ_{xy} is of order ten times larger in the amorphous samples than in the crystalline ones, similar to the difference in ρ_{xx}. A similar difference in ρ_{xy} is seen between epitaxial samples with $D0_3$ and B2 structures. By instead considering the anomalous Hall *conductivity* σ_{xy} and suitably normalizing by M_z and $n_h^{2/3}$ the AHE is roughly constant *for all samples*, suggesting a primary dependence of the AHE on the intrinsic mechanism. A comparable scaling is observed in GaMnAs films, although σ_{xy} normalized by M_z and $n_h^{2/3}$ is nearly two orders of magnitude larger; we attribute this to differences in local coupling J_{pd}. Our result is quite remarkable for the amorphous samples, which lack lattice periodicity, since the intrinsic mechanism originates from Berry phase curvature, suggesting that local structure as opposed to global symmetries plays the central role in the origin of AHE.

* * *

This work was supported by the US Department of Energy, Office of Science, Basic Energy Sciences, Materials Sciences and Engineering Division. We gratefully thank W. A. Saslow and A. Kowalewski for enlightening discussions and D. Mendinueto for help with transport measurements.

REFERENCES

[1] Qi X. L. and Zhang S. C., *Rev. Mod. Phys.*, **83** (2011) 1057.
[2] Bernevig B. A., Hughes T. L. and Zhang S. C., *Science*, **315** (2006) 1757.
[3] Wan X., Turner A. M., Vishwanath A. and Savrasov S. Y., *Phys. Rev. B*, **83** (2011) 205101.
[4] Yang K.-Y., Lu Y.-M. and Ran Y., *Phys. Rev. B*, **84** (2011) 075129.
[5] Burkov A. A. and Balents L., *Phys. Rev. Lett.*, **107** (2011) 127205.
[6] Xiao D., Chang M.-C. and Niu Q., *Rev. Mod. Phys.*, **82** (2010) 1959.
[7] Nagaosa N., Sinova J., Onoda S., MacDonald A. H. and Ong N. P., *Rev. Mod. Phys.*, **82** (2010) 1539.

[8] Onoda S., Sugimoto N. and Nagaosa N., *Phys. Rev. Lett.*, **97** (2006) 126602.
[9] Smit J., *Physica*, **21** (1955) 877.
[10] Smit J., *Physica*, **24** (1958) 39.
[11] Xiao D., Chang M.-C. and Niu Q., *Rev. Mod. Phys.*, **82** (2010) 1959.
[12] Shiomi Y., Onose Y. and Tokura Y., *Phys. Rev. B*, **79** (2009) 100404.
[13] Miyasato T., Abe N., Fujii T., Asamitsu A., Onoda S., Onose Y., Nagaosa N. and Tokura Y., *Phys. Rev. Lett.*, **99** (2007) 086602.
[14] Schad R., Beliën P., Verbanck G., Moshchalkov V. V. and Bruynseraede Y., *J. Phys.: Condens. Matter*, **10** (1998) 6643.
[15] Lee W.-L., Watauchi S., Miller V. L., Cava R. J. and Ong N. P., *Science*, **303** (2004) 1647.
[16] Hsu H. S., Lin C. P., Sun S. J. and Chou H., *Appl. Phys. Lett.*, **96** (2010) 242507.
[17] Toyosaki H., Fukumura T., Yamada Y., Nakajima K., Chikyow T., Hasegawa T., Koinuma H. and Kawasaki M., *Nat. Mater.*, **3** (2004) 221.
[18] Venkateshvaran D., Kaiser W., Boger A., Althammer M., Ramachandra Rao M. S., Goennenwein S. T. B., Opel M. and Gross R., *Phys. Rev. B*, **78** (2008) 092405.
[19] Karel J., Zhang Y. N., Bordel C., Stone K. H., Jenkins C. A., Smith David J., Hu J., Wu R. Q. and Heald S. M., Kortright J. B. and Hellman F., *Mater. Res. Express*, **1** (2014) 026102.
[20] Karel J., Juraszek J., Minar J., Bordel C., Stone K. H., Zhang Y. N., Hu J., Wu R. Q., Ebert H., Kortright J. B. and Hellman F., *Phys. Rev. B*, **91** (2015) 144402.
[21] Mooij J. H., *Phys. Status Solidi (A)*, **17** (1973) 521.
[22] Tsuei C. C., *Phys. Rev. Lett.*, **57** (1986) 1943.
[23] Kondo J., *Prog. Theor. Phys.*, **32** (1964) 37.
[24] Fawcett E., Alberts H. L., Galkin V. Yu., Noakes D. R. and Yakhmi J. V., *Rev. Mod. Phys.*, **66** (1994) 25.
[25] McGuire T. R. and Potter R. I., *IEEE Trans. Magn.*, **11** (1975) 1018.
[26] Bergmann G., *Phys. Rep.*, **107** (1984) 1.
[27] Mangin Ph. and Marchal G., *J. Appl. Phys.*, **49** (1978) 1709.
[28] Foner S., *Phys. Rev.*, **107** (1957) 1513.
[29] Kobayashi Y., Kaneko T., Kamogawa M., Asai K., Akiyama K. and Funakubo H., *J. Phys. D: Appl. Phys.*, **40** (2007) 6873.
[30] Raeburn S. J. and Aldridge R. V., *J. Phys. F: Met. Phys.*, **8** (1978) 1917.
[31] Manyala N., Sidis Y., DiTusa J. F., Aeppli G., Young D. P. and Fisk Z., *Nat. Mater.*, **3** (2004) 255.
[32] Chun S. H., Kim Y. S., Choi H. K., Jeong I. T., Lee W. O., Suh K. S., Oh Y. S., Kim K. H., Khim Z. G., Woo J. C. and Park Y. D., *Phys. Rev. Lett.*, **98** (2007) 026601.
[33] Weischenberg J., Freimuth F., Sinova J., Blügel S. and Mokrousov Y., *Phys. Rev. Lett.*, **107** (2011) 106601.
[34] Pu Y., Chiba D., Matsukura F., Ohno H. and Shi J., *Phys. Rev. Lett.*, **101** (2008) 117208.